Theoretical study on the mechanism of a ring-opening reaction of oxirane by the active-site aspartic dyad of HIV-1 protease†

Juraj Kóňa*[a,b]

Received 15th October 2007, Accepted 8th November 2007
First published as an Advance Article on the web 6th December 2007
DOI: 10.1039/b715828a

Two possible mechanisms of the irreversible inhibition of HIV-1 protease by epoxide inhibitors are investigated on an enzymatic model using *ab initio* (MP2) and density functional theory (DFT) methods (B3LYP, MPW1K and M05-2X). The calculations predict the inhibition as a general acid-catalyzed nucleophilic substitution reaction proceeding by a concerted S_N2 mechanism with a reaction barrier of *ca.* 15–21 kcal mol^{-1}. The irreversible nature of the inhibition is characterized by a large negative reaction energy of *ca.* −17–(−24) kcal mol^{-1}. A mechanism with a direct proton transfer from an aspartic acid residue of the active site onto the epoxide ring has been shown to be preferred compared to one with the proton transfer from the acid catalyst facilitated by a bridging catalytic water molecule. Based on the geometry of the transition state, structural data important for the design of irreversible epoxide inhibitors of HIV-1 protease were defined. Here we also briefly discuss differences between the epoxide ring-opening reaction in HIV-1 protease and epoxide hydrolase, and the accuracy of the DFT method used.

Introduction

Human immunodeficiency virus 1 (HIV-1) retropepsin, more commonly known as HIV-1 protease (HIV-1 PR) is an aspartic peptidase essential in the proper assembly and maturation of infectious virions.[1] The biological activity of HIV-1 PR is to separate ten asymmetric and nonhomologous sequences in the Gag and Pol polyproteins.[2–4] The HIV-1 PR dimer consists of two identical, noncovalently associated subunits of 99 amino acid residues, in which each monomer contributes one conserved Asp-Thr-Gly triad to the pseudo-symmetric active site.[5] The catalytic mechanism of HIV-1 PR is consistent with a general acid–base mechanism, in which the two active site aspartate residues (Asp25 and Asp25′) play an essential general acid–base role in activating the water molecule that acts as a nucleophile and attacks the carbonyl carbon of the scissile peptide bond.[6] The pH–rate profile of this enzyme implies that only one of the two active site aspartic acids is unprotonated in the active pH range.[7–10] Based on X-ray crystallography,[11] theoretical,[12–14] kinetic and affinity labeling studies,[8,15] the catalytic mechanism has been established as a stepwise addition–elimination substitution, which takes place through an oxyanion tetrahedral intermediate during the rate-determining elimination step.

Designing drugs for HIV infection is today one of the largest collective efforts of the scientific community.[16] Since HIV-1 PR is essential to viral maturation, it has become a logical target for AIDS therapy.[2,17,18] Although several inhibitors of HIV-1 PR are already in use or in clinical trials as anti-HIV drugs,[16] their effectiveness is hampered by the emergence of drug-resistant variants, many of which are widely cross-resistant.[19–21]

Calorimetric measurements[22–24] of the binding thermodynamics of several first- and second-generation inhibitors have shown that their binding affinities are dominated by an extremely large positive entropy of solvation (high hydrophobicity) and a minimal loss of conformational entropy (rigidity of inhibitors) that overcome their unfavorable or only slightly favorable binding enthalpies. Therefore, one strategy for the development of a new generation of HIV-1 PR inhibitors is to optimize their binding affinities towards more favorable binding enthalpies (more flexible inhibitors) during the initial stages of the design process.[25,26] Another strategy for minimizing drug resistance is to develop irreversible rather than reversible inhibitors of HIV-1 PR.[27–37] Irreversible inhibitors are less sensitive to mutations because even a low degree of active-site occupancy can lead in time to complete inactivation of the protein. The catalytic aspartate residues are the ideal target for such irreversible inhibitors, because their mutation results in the complete loss of catalytic activity.[38] Irreversible inhibition of HIV-1 PR was first achieved with 1,2-epoxy-3-(*p*-nitrophenoxy)propane (EPNP),[7] a small epoxide molecule that is a general irreversible inhibitor of aspartyl proteases (Fig. 1).[39,40] Mass spectrometric analysis of the inactivated enzyme shows that one molecule of EPNP is covalently bound to a catalytic aspartate residue per HIV-1 PR dimer.[27] EPNP is a nonspecific and relatively weak irreversible inhibitor of HIV-1 PR, HIV-2 PR and simian immunodeficiency virus protease (SIV PR) (K_{inact} = 6.7–9.9 mM, V_{inact} = 48–60 × 10^{-3} min^{-1}).[35,41] In an effort to develop epoxide-containing irreversible inhibitors with high potency, non-peptide[27] and peptidomimetic inhibitors of HIV-1 PR containing a *cis*-epoxide were designed, synthesized and kinetically characterized

[a]*International School for Advanced Studies (SISSA) and Democritos Modeling Center for Research in Atomistic Simulation (INFM), via Beirut 2-4, 34014 Trieste, Italy*
[b]*Institute of Chemistry, Center for Glycomics, Slovak Academy of Sciences, Dúbravska cesta 9, SK-845 38 Bratislava, Slovak Republic. E-mail: chemkona@savba.sk; Fax: +421-2-59410222; Tel: +421-2-59410203*

† Electronic supplementary information (ESI) available: Table of total energies including ZPE corrections and thermal corrections to Gibbs free energy, as well as Cartesian coordinates of the B3LYP and M05-2X optimized structures. See DOI: 10.1039/b715828a

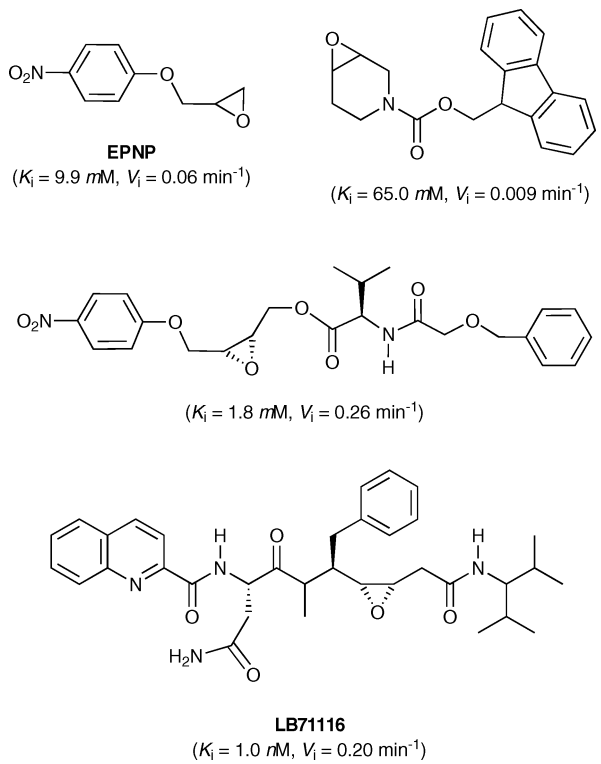

Fig. 1 Schematic structures of EPNP, non-peptide and peptidomimetic inhibitors of HIV-1 PR.

(Fig. 1).[28–30] However, in order to further improve their irreversible potency, structural characterization of the transition states of their inhibition reactions in a three dimensional structure of HIV-1 PR will be required and quantum mechanical (QM) calculations can be very helpful in shedding some light on these issues.

The mechanism of the irreversible inhibition of HIV-1 PR by non-peptide epoxide inhibitors has been studied by Mavri[42] on small organic models using semi-empirical and QM methods. The calculations suggest that the reaction is specific for the catalytic aspartic acid residues, and for effective inhibition the participation of both residues, one as a nucleophile and the other as a general acid catalyst, is essential (Fig. 2). The general acid-catalyzed mechanism was also proposed by theoretical studies on analogous enzymatic reactions in epoxide hydrolases[43–47] and the irreversible inhibition of glycosidases.[48] Detailed mechanistic and energetic properties of the ring-opening reaction of simple epoxides by oxygen, nitrogen and sulfur nucleophiles were investigated by QM[49–57] and semi-empirical methods.[57,58] However, for the correct modeling of such a reaction at the HIV-1 PR active site, much larger models than the commonly used acetic acid–acetate moieties are required.[59,60] To describe electrostatic interactions and hydrogen bonds correctly, the modeling by QM calculations should take into account the active-site residues Asp25 to Ala28.[59]

In this study, we modeled two possible mechanisms for the irreversible inhibition of HIV-1 PR by epoxides, including in calculations a large quantum cluster of the active site (Fig. 3). In mechanism A, a general acid-catalyzed nucleophilic substitution with a direct proton transfer from the catalytic aspartic acid residue onto the epoxide ring is modeled (Fig. 2). The reaction catalyzed by a proton transfer involving a bridging catalytic water molecule is also investigated (mechanism B). Finally, based on the geometry of the transition state, structural data important for the design of irreversible epoxide inhibitors of HIV-1 PR were defined. Here we also briefly discuss differences between the epoxide ring-opening reaction in HIV-1 PR and epoxide hydrolase, and the accuracy of the B3LYP method used.

Computational details

Methods

Calculations were performed using the Hartree–Fock method (HF)[61] with the Pople's split valence double-ζ basis set[62–64] augmented by polarization functions on all atoms except for hydrogens [6-31G(d)], the second-order Møller–Plesset theory (MP2),[65–68] the local MP2 (LMP2),[65,69,70] with two hybrid generalized gradient approximation (GGA) density functionals: Becke's three-parameter exchange functional with the Lee–Yang–Parr correlation functional (B3LYP)[71–73] and the Perdew–Wang exchange functional combined with the Perdew–Wang-1991 correlation functional modified for kinetics (MPW1K),[74–77] and with the hybrid meta-GGA M05-2X functional[78–80] with the 6-31+G(d,p) basis set augmented by polarization functions on all atoms and diffuse functions on all atoms except for hydrogens. The hybrid MP2/6-31+G(d,p):HF/6-31G(d) and B3LYP/6-31+G(d,p):HF/6-31G(d) scan calculations were performed using the Gaussian 03 program.[81] The optimization, frequency and single point calculations at the DFT and LMP2 levels were performed with the Jaguar 7 program[82] (for more details see the Active-site model and Geometry optimization subsections). The restricted formalism was used for all calculations (preliminary calculations of **TSA** optimized at the unrestricted B3LYP level gave identical geometry compared to the restricted B3LYP calculations. The difference in UB3LYP and RB3LYP energies was *ca.* 0.09 kcal mol^{-1}).

Active-site model

Based on a crystal structure of HIV-1 PR co-crystallized with a non-peptide inhibitor (PDB ID:1AID),[83] an active site model was built from residues located within a radius of *ca.* 7 Å from the reaction center of an epoxide inhibitor (Fig. 3). As was mentioned above,[59] the active-site residues from Asp25 to Ala28 should be taken into account for correct modeling of the electrostatic interactions and hydrogen bonds in the active site, and the reactivity and acidic properties of the catalytic nucleophile and acid. The model consisting of a hexapeptide dimer with terminal acetyl (Ace) and *N*-methylamino groups (Nme) (Ace-Asp25-Thr26-Gly27-Ala28-Nme and Ace-Asp25′-Thr26′-Gly27′-Ala28′-Nme), an inhibitor (oxirane) and a catalytic water molecule, was divided into two QM layers (QM1:QM2) using the ONIOM method.[84–86] The oxirane, water molecule and side chains of the Asp25 and Asp25′ catalytic residues were treated at the QM1 level and the rest of the enzymatic model at the QM2 level. Consequently for reaction path calculations, two ONIOM schemes, QM1[MP2/6-31+G(d,p)]:QM2[HF/6-31G(d)] and QM1[B3LYP/6-31+G(d,p)]:QM2[HF/6-31G(d)], were calculated for the above-mentioned mechanisms A and B using the Gaussian 03 program.[81] In all, the quantum cluster comprised of 118 atoms [QM1(20 atoms) + QM2(98 atoms)]

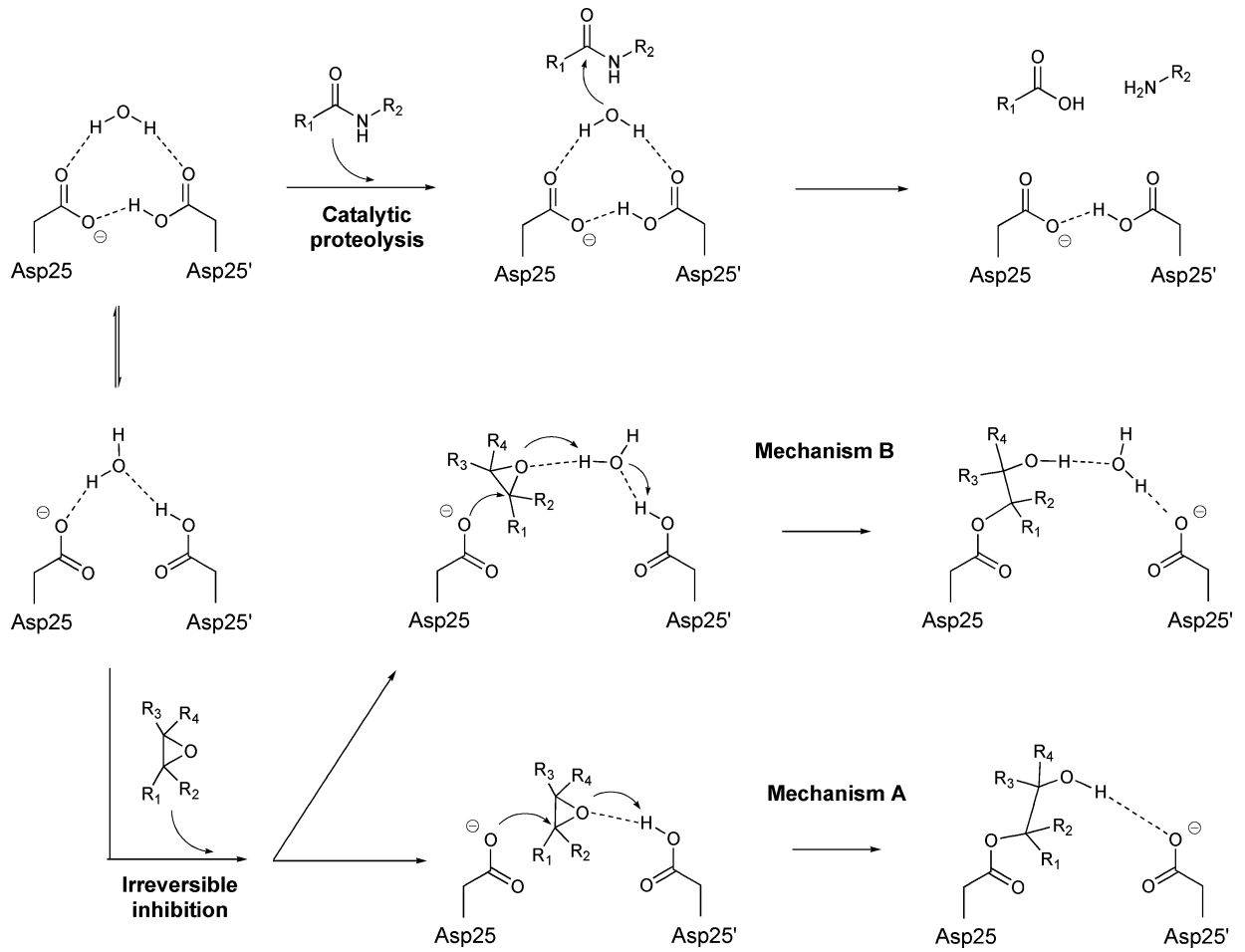

Fig. 2 Schematic mechanisms of the catalytic proteolysis of a native substrate and the irreversible inhibition by an epoxide inhibitor.

for the mechanism A and 121 atoms [QM1(23 atoms) + QM2(98 atoms)] for the mechanism B.

Geometry optimization

During geometry optimization, some degrees of freedom were constrained to maintain a reasonable approximation to the active site geometry of the HIV-1 protease. The four terminal carbons of the Ace and Nme residues were fixed according to the crystal structure.[83] In mapping the potential energy surface (PES) of the reaction, a scan procedure on the two ONIOM schemes was performed along an O3–C5 reaction coordinate (the O3 oxygen of the carboxylate side chain of Asp25 and the C5 carbon of the oxirane, see atom numbering in Fig. 3) stepped by 0.1 Å with remaining coordinates optimized, subject to the above-mentioned constraints. Then, the geometries of all minima on the PES were fully optimized with no constraints on the O3–C5 distance by means of the Berny algorithm using redundant internal coordinates.[87] Preliminary structures of the transition states were refined by an additional scan procedure stepped by 0.01 Å.

For the mechanism A (which has been shown to be the preferable one) full optimizations of an initial complex, transition state and covalent enzyme–inhibitor intermediate were performed at the B3LYP/6-31+G(d,p) level using the geometries from the ONIOM scan calculations. All stationary points were characterized as either minima or transition states by vibrational frequency calculations. The transition state **TSA** was verified as having one large imaginary frequency (*ca.* i605.6 cm^{-1}). Fixing some atoms in their crystallographically observed positions gives rise to a few small negative imaginary frequencies for the optimized structures. These are, however, very small, in the order of −10 to −60 cm^{-1}, and do not affect the obtained results. Thermodynamic quantities were calculated at 298 K and 101.325 kPa using standard rigid-rotor and harmonic oscillator partition function expressions. Zero-point corrections and thermal corrections to enthalpy and Gibbs free energies were calculated from unscaled frequencies obtained at the same level as the geometry optimizations. Solvent effects (aqueous solution, $\varepsilon = 80.4$, probe radius 1.4) were estimated by single-point calculations using Jaguar's Poisson–Boltzmann self-consistent reaction field model (PB-SCRF)[88–90] at the B3LYP/6-31+G(d,p) level. The effective local dielectric constant in the enzyme may vary strongly depending on the local environment. A dielectric constant of 80 would be equivalent to a completely solvent exposed site. Thus, by calculating free energy differences both in the gas phase ($\varepsilon = 1.0$) and in aqueous solution the two extrema in solvent effects are represented.

In addition, the accuracy of the B3LYP energies was tested by single point calculations at the MPW1K/6-31+G(d,p)//B3LYP/6-31+G(d,p), M05-2X/6-31+G(d,p)//B3LYP/6-31+G(d,p) and

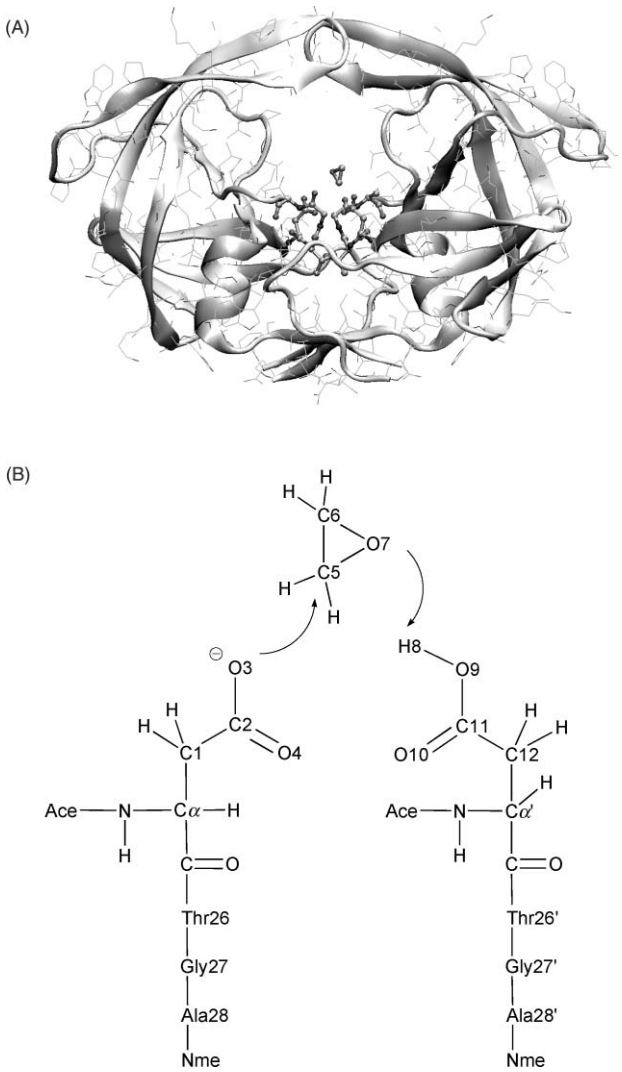

Fig. 3 An active-site model with oxirane and the catalytic site visualized by ball & stick (hydrogen atoms are omitted for the sake of clarity) in a 3D structure of HIV-1 PR (above), and the numbering of selected atoms of the calculation cluster (below).

LMP2/6-31+G(d,p)//B3LYP/6-31+G(d,p) levels using the Jaguar 7 program,[82] where thermal and solvent corrections were added from the above-mentioned B3LYP and PB-SCRF-B3LYP calculations.

Results and discussion

From scan calculations at the ONIOM[MP2/6-31+G(d,p):HF/6-31G(d)] and ONIOM[B3LYP/6-31+G(d,p):HF/6-31G(d)] levels preliminary structures of transition states **TSA** and **TSB**, and their activation energies were calculated (Fig. 4). As summarized in Table 1 the activation energy of mechanism A is *ca.* 4–7 kcal mol^{-1} lower compared to that of mechanism B. Consequently, mechanism B was not considered further, and full geometry refinements of stationary points at the B3LYP/6-31+G(d,p) level were only performed on the structures of mechanism A.

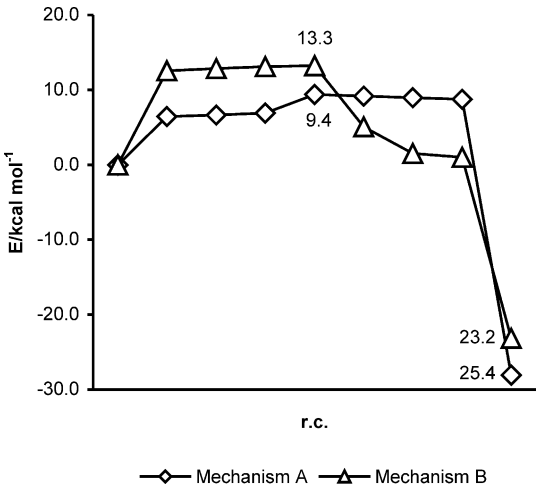

Fig. 4 Energy profiles (in kcal mol^{-1}) of mechanisms A and B calculated at the ONIOM[B3LYP/6-31+G(d,p):HF/6-31G(d)] level from the scan procedure stepped by 0.01 Å.

The transition state **TSA** of an attack by the nucleophile (the O3 oxygen of the ionized Asp25 residue) on the C5 carbon of the oxirane was localized at a distance d(O3–C5) = 2.17 Å. As shown in Fig. 5, in the transition state the oxirane ring is partially opened [d(C5–O7) = 1.77 Å] with the O7 leaving oxygen partially protonated by the other catalytic aspartate residue (protonated Asp25′) [d(O7–H8) = 1.18 Å and d(H8–O9) = 1.24 Å]. The **TSA** was verified by a vibrational frequency calculation with one large imaginary frequency (ν_i = i605.6 cm^{-1}) belonging to the breaking–forming of bonds (O3–C5, C5–O7, O7–H8, H8–O9). The minimization calculations starting from **TSA** resulted in a starting complex **1A** and a covalent intermediate **2A** (Cartesian coordinates of all the stationary points are available in the ESI†).

Table 1 Relative energies (ΔE_0) including ZPE corrections (ΔE) and Gibbs free energies (ΔG) of minima and transition states of mechanisms A and B in the gas phase and in aqueous solution (ΔG_{aq}) in kcal mol^{-1} (for total energies, see ESI†)

	ΔE_0[a]	ΔE_0[b]	ΔE[c]	ΔG[c]	ΔG_{aq}[c]	ΔG_{aq}[d]	ΔG_{aq}[e]	ΔG_{aq}[f]
1A	0.0	0.0	0.0	0.0	0.0	0.0	0.0	0.0
TSA	11.4	9.4	9.0	12.5	15.0	17.9	14.2	21.4
2A	−25.6	−25.4	−26.6	−21.7	−18.2	−21.3	−23.9	17.0
1B	0.0	0.0						
TSB	17.9	13.3						
2B	−23.0	−23.2						

[a] QM1[MP2/6-31+G(d,p)]:QM2[HF/6-31G(d)]. [b] QM1[B3LYP/6-31+G(d,p)]:QM2[HF/6-31G(d)]. [c] B3LYP/6-31+G(d,p)//B3LYP/6-31+G(d,p). [d] MPW1K/6-31+G(d,p)//B3LYP/6-31+G(d,p). [e] M05-2X/6-31+G(d,p)//B3LYP/6-31+G(d,p). [f] LMP2/6-31+G(d,p)//B3LYP/6-31+G(d,p).

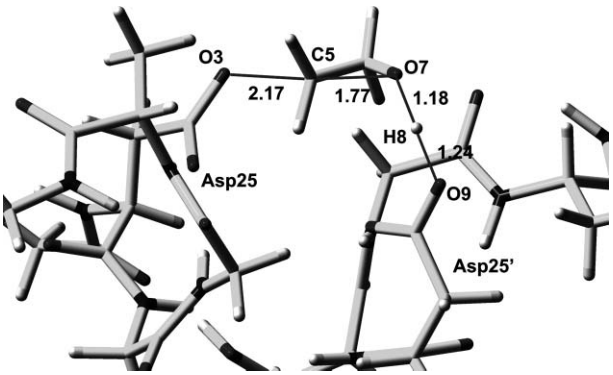

Fig. 5 B3LYP optimized transition state **TSA** with selected distances (in Å). Some hydrogen atoms are omitted for the sake of clarity.

The reaction path **1A** → **TSA** → **2A** is predicted as a general acid-catalyzed nucleophilic substitution proceeding by the S_N2 mechanism, in which addition of the nucleophile, elimination of the leaving group (fission of the oxirane ring) and proton transfer from the acid catalyst take place in a concerted manner. The activation barrier of the inhibition reaction ($\Delta G^{\ddagger}$) ranges from 12.5 (gas phase, B3LYP) to 15.0 kcal mol^{-1} (aqueous solution, PB-B3LYP) (Fig. 6 and Table 1). It is known that the B3LYP method tends to underestimate reaction barrier heights and has a mean unsigned error (MUE) of *ca.* 3–5 kcal mol^{-1}.[74,75,77–79,91] Therefore, we compared the accuracy of the B3LYP results with those obtained by the MPW1K, M05-2X and MP2 methods. The MPW1K functional was developed for accurate prediction of the thermochemical kinetics with a MUE of *ca.* 1.5 kcal mol^{-1}.[74,75] The recently developed M05-2X functional provides calculations with similar accuracy (MUE of 1.9 kcal mol^{-1})[79] and was recommended for epoxide structures by Zhao and Truhlar.[92] The M05-2X functional gave for our inhibition reaction a similar activation barrier of 14.2 kcal mol^{-1}, and MPW1K and LMP2 results were 3–5 kcal mol^{-1} higher compared to the B3LYP method. The calculated barriers are quantitatively in reasonable agreement with experimentally available inhibition rates of epoxide inhibitors

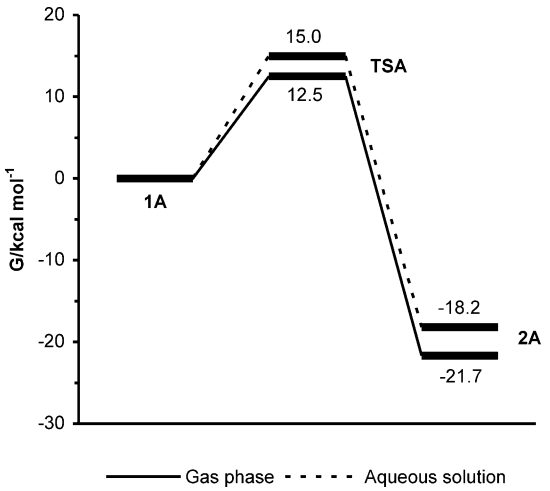

Fig. 6 Energy profiles (in kcal mol^{-1}) of mechanism A calculated in the gas phase [B3LYP/6-31+G(d,p)//B3LYP/6-31+G(d,p)] and in aqueous solution [PB-B3LYP/6-31+G(d,p)//B3LYP/6-31+G(d,p)].

($V_i = 10^{-1}$–10^{-3} s^{-1}, corresponding to activation barriers of *ca.* 15–20 kcal mol^{-1}).[27–29,31,35,39–41] The irreversible nature of the inhibition is demonstrated by the large negative value of the reaction energy of *ca.* −17–(−24) kcal mol^{-1}. The reaction step of the irreversible inhibition of HIV-1 PR by epoxides is analogous to the first catalytic step of epoxide hydrolases. We compared our reaction profile with that of a ring-opening reaction of a *trans*-substituted epoxide catalyzed by soluble epoxide hydrolase (EH) calculated by Hopmann and Himo.[44,45] The B3LYP activation barrier of *ca.* 8 kcal mol^{-1} for EH is similar to that for HIV-1 PR, but the reaction energies are significantly more negative for HIV-1 PR (−8 kcal mol^{-1} in EH *versus* −18 kcal mol^{-1} in HIV-1 PR). This explains why HIV-1 PR can bind the epoxide inhibitors in an irreversible manner. In EH two tyrosines play the role of the catalytic acid. They are, in general, weaker acids (pK_a *ca.* 10.0) compared with the Asp residues (pK_a *ca.* 4.0). The strength of the catalytic acid also influences mechanistic aspects of the reaction. While in HIV-1 PR the ring-opening and proton transfer reactions take place in a concerted manner, in EH the reaction steps proceed by a stepwise mechanism.

The water molecule, which plays a vital role in the proteolytic reaction catalyzed by HIV-1 PR (Fig. 2), has been shown to be not crucial for irreversible epoxide inhibition. The mechanism B, in which the oxirane-ring fission was facilitated by the acid catalyst (Asp25′) through a water bridge, is energetically less preferable. The most feasible inhibition is carried out with the direct participation of the acidic catalyst. Due to the specific position of the catalytic aspartic dyad of HIV-1 PR, they can work as cooperative nucleophile–acid machinery for fission of the epoxide ring of the inhibitors. It should be emphasized that the carboxylate ion is a weak nucleophile, and the assistance of the other Asp residue, as a general acid catalyst, is essential for the irreversible epoxide inhibition.[42,48] As was demonstrated by DFT calculations,[42,44,47,48] the ring opening of epoxides has a significantly high activation barrier of *ca.* 15–25 kcal mol^{-1} without involving the catalytic acid in the reaction system. Thus for efficient reaction, the epoxide ring must fit a specific binding position in the active site of HIV-1 PR, which can be characterized by the geometric parameters of the transition state **TSA** defined in Tables 2 and 3. A detailed structural analysis of **TSA** (Fig. 5) reveals that only mono substituted and *cis*-1,2-disubstituted epoxides are preferable configurations. The *trans* or 1,1-disubstituted configurations of the epoxide ring would hinder the proper orientation of the ring necessary for the proton transfer from Asp25′ onto the ring oxygen of the inhibitor. This is in agreement with observations that only

Table 2 Selected geometric parameters of the minima and the transition state optimized at the B3LYP/6-31+G(d,p) and M05-2X/6-31+G(d,p) (values in brackets) levels: the distances (d) in Å, valence angles (η), and torsion angles (ϕ) in degrees (for other data, see 3D structures in ESI†)

	1A	TSA	2A
d(O3–C5)	3.06	2.17 (2.11)	1.47
d(C5–O7)	1.47	1.77 (1.78)	2.41
d(O7–H8)	1.58	1.18 (1.10)	0.99
d(H8–O9)	1.02	1.24 (1.35)	1.75
η(C2–O3–C5)	96.7	111.9 (111.2)	119.1
η(O3–C5–C6)	110.0	105.8 (108.6)	108.0
ϕ(C1–C2–O3–C5)	−140.8	−165.3 (−169.6)	−179.3
ϕ(C2–O3–C5–C6)	77.8	129.9 (133.0)	137.5

Table 3 Selected structural parameters—interatomic distances (in Å) and angles (in degrees) among noncovalently associated atoms—in the **TSA** transition state optimized by the B3LYP and M05-2X methods (for other data, see 3D structures in ESI†)

	B3LYP	M05-2X
d(Cα–C5)	5.24	5.34
d(Cα–C6)	5.90	6.28
d(Cα′–O7)	5.83	5.70
d(Cα′–C5)	6.07	5.72
ϕ(Cα–C1–C5–C6)	81.6	103.5
ϕ(Cα–C1–C5–O7)	39.7	45.9
ϕ(Cα′–C12–O7–C5)	22.3	2.2
ϕ(Cα′–C12–O7–C6)	−31.2	−50.1

compounds with the *cis* configuration of the epoxide ring are potent irreversible inhibitors of HIV-1 PR.[27–31]

Recently it was demonstrated that the B3LYP functional can correctly describe the geometries of simple epoxide oxonium ions[93] except for asymmetrically substituted derivatives.[94] Zhao and Truhlar recommend using a new functional M05-2X, which gives the right bond length for the problematic C–O bond of the protonated epoxide ring.[92] To verify the accuracy of the B3LYP geometry of the transition state, we re-calculated **TSA** at the M05-2X/6-31+G(d,p) level. As can be seen in Table 2 (values in brackets), the new optimized geometry is close to that of B3LYP with a difference of 0.01 Å for the C–O bond. However, some discrepancies can be seen in the torsion angles among noncovalently associated atoms of the cluster (Table 3), where B3LYP and M05-2X values differ by *ca.* 20°. In addition, we also compared our geometry of the transition state with those calculated for epoxide ring opening by HIV-1 PR[42] and other enzymatic systems such as EH[44–46] and glycosylhydrolases.[48] Again, we found good agreement in the bond lengths for the breaking–forming bonds [differences for d(O3–C5) of *ca.* 0.07 Å and d(C5–O7) of *ca.* 0.09 Å].

Conclusion

We investigated at the quantum chemical level the structural and energetic properties of the reaction between the active-site cluster of HIV-1 PR and oxirane as a model for the irreversible inhibition of the enzyme by epoxide inhibitors. The main goal was to understand the irreversible nature of the reaction and define a geometry of the transition state. The methods predict the inhibition as occurring by a general acid-catalyzed nucleophilic substitution reaction proceeding by a concerted S_N2 mechanism. The one ionized Asp residue acts as a nucleophile attacking the electrophilic carbon at the oxirane ring and the other protonated Asp residue plays the role of a general acid catalyst facilitating the ring fission of the inhibitor by transferring a proton onto the oxygen of the oxirane ring. Mechanism A, with direct proton transfer from the acid catalyst to the inhibitor, is predicted as the most feasible process with an activation barrier of *ca.* 15–21 kcal mol^{-1}. The irreversible nature of the inhibition is demonstrated by the large negative value of the reaction energy of *ca.* −17–(−24) kcal mol^{-1}. The main difference between the irreversible epoxide ring opening in HIV-1 PR and the reversible opening in EH is in the strength of the assisting catalytic acid (Asp *versus* Tyr) and in the way the proton transfer occurs (concerted *versus* stepwise mechanism).

From a detailed 3D analysis of the transition state, inhibitors with mono substituted and *cis*-1,2-disubstituted epoxide rings are preferable for a covalent interaction with the aspartic dyad of HIV-1 PR. A potent inhibitor should bind into the active site at a position which allows the oxygen of the epoxide ring to be easily protonated by the active-site aspartic acid [Φ(Cα′–C12–O7–C5) = 10° ± 10 and Φ(Cα′–C12–O7–C6) = −40° ± 10].

Acknowledgements

We thank the computer center CINECA Bologna and Dr Tvaroška for support with the Gaussian and Jaguar calculations.

References

1 B. M. Dunn and M. Rao, in *Handbook of Proteolytic Enzymes*, ed. A. J. Barrett, N. D. Rawlings and J. F. Woessner, Elsevier Academic Press, Amsterdam, 2004, vol. 1, pp. 144–157.
2 J. W. Erickson, in *Protease inhibitors in AIDS therapy*, ed. R. C. Ogden and C. W. Flexner, Marcel Dekker, New York, 2001, pp. 1–27.
3 M. Prabu-Jeyabalan, E. Nalivaika and C. A. Schiffer, *Structure*, 2002, **10**, 369–381.
4 M. Prabu-Jeyabalan, E. Nalivaika and C. A. Schiffer, *J. Mol. Biol.*, 2000, **301**, 1207–1220.
5 J. Vondrasek and A. Wlodawer, *Proteins*, 2002, **49**, 429–431.
6 A. Brik and C. H. Wong, *Org. Biomol. Chem.*, 2003, **1**, 5–14.
7 T. D. Meek, B. D. Dayton, B. W. Metcalf, G. B. Dreyer, J. E. Strickler, J. G. Gorniak, M. Rosenberg, M. L. Moore, V. W. Magaard and C. Debouck, *Proc. Natl. Acad. Sci. U. S. A.*, 1989, **86**, 1841–1845.
8 L. J. Hyland, T. A. Tomaszek and T. D. Meek, *Biochemistry*, 1991, **30**, 8454–8463.
9 S. K. Grant, I. C. Deckman, M. D. Minnich, J. Culp, S. Franklin, G. B. Dreyer, T. A. Tomaszek, C. Debouck and T. D. Meek, *Biochemistry*, 1991, **30**, 8424–8434.
10 T. Hofmann, R. S. Hodges and M. N. G. James, *Biochemistry*, 1984, **23**, 635–643.
11 A. Wlodawer and A. Gustchina, *Biochim. Biophys. Acta, Protein Struct. Mol. Enzymol.*, 2000, **1477**, 16–34.
12 S. Piana, D. Bucher, P. Carloni and U. Rothlisberger, *J. Phys. Chem. B*, 2004, **108**, 11139–11149.
13 H. Y. Liu, F. MullerPlathe and W. F. vanGunsteren, *J. Mol. Biol.*, 1996, **261**, 454–469.
14 H. Park, J. Suh and S. Lee, *J. Am. Chem. Soc.*, 2000, **122**, 3901–3908.
15 L. J. Hyland, T. A. Tomaszek, G. D. Roberts, S. A. Carr, V. W. Magaard, H. L. Bryan, S. A. Fakhoury, M. L. Moore, M. D. Minnich, J. S. Culp, R. L. Desjarlais and T. D. Meek, *Biochemistry*, 1991, **30**, 8441–8453.
16 A. Wlodawer, *Annu. Rev. Med.*, 2002, **53**, 595–614.
17 A. Wlodawer and J. Vondrasek, *Annu. Rev. Biophys. Biomol. Struct.*, 1998, **27**, 249–284.
18 A. Wlodawer and J. W. Erickson, *Annu. Rev. Biochem.*, 1993, **62**, 543–585.
19 D. Boden and M. Markowitz, *Antimicrob. Agents Chemother.*, 1998, **42**, 2775–2783.
20 R. W. Shafer, M. A. Winters, S. Palmer and T. C. Merigan, *Ann. Intern. Med.*, 1998, **128**, 906–911.
21 F. Wartha, A. H. C. Horn, H. Meiselbach and H. Sticht, *J. Chem. Theory Comput.*, 2005, **1**, 315–324.
22 A. Velazquez-Campoy, M. J. Todd and E. Freire, *Biochemistry*, 2000, **39**, 2201–2207.
23 M. J. Todd, I. Luque, A. Velazquez-Campoy and E. Freire, *Biochemistry*, 2000, **39**, 11876–11883.
24 A. Velazquez-Campoy, Y. Kiso and E. Freire, *Arch. Biochem. Biophys.*, 2001, **390**, 169–175.
25 H. Ohtaka, S. Muzammil, A. Schon, A. Velazquez-Campoy, S. Vega and E. Freire, *Int. J. Biochem. Cell Biol.*, 2004, **36**, 1787–1799.
26 W. Wang and P. A. Kollman, *Proc. Natl. Acad. Sci. U. S. A.*, 2001, **98**, 14937–14942.

27 Z. H. Yu, P. Caldera, F. McPhee, J. J. De Voss, P. R. Jones, A. L. Burlingame, I. D. Kuntz, C. S. Craik and P. R. Ortiz de Montellano, *J. Am. Chem. Soc.*, 1996, **118**, 5846–5856.
28 C. H. Park, J. S. Koh, Y. C. Son, H. I. Choi, C. S. Lee, N. Y. Choy, K. Y. Moon, W. H. Jung, S. C. Kim and H. S. Yoon, *Bioorg. Med. Chem. Lett.*, 1995, **5**, 1843–1848.
29 C. S. Lee, N. Choy, C. Park, H. Choi, Y. C. Son, S. Kim, J. H. Ok, H. Yoon and S. C. Kim, *Bioorg. Med. Chem. Lett.*, 1996, **6**, 589–594.
30 N. Choy, H. I. Choi, W. H. Jung, C. R. Kim, H. Yoon, S. C. Kim, T. G. Lee and J. S. Koh, *Bioorg. Med. Chem. Lett.*, 1997, **7**, 2635–2638.
31 S. K. Grant, M. L. Moore, S. A. Fakhoury, T. A. Tomaszek and T. D. Meek, *Bioorg. Med. Chem. Lett.*, 1992, **2**, 1441–1445.
32 A. Albeck, *Drug Dev. Res.*, 2000, **50**, 425–434.
33 A. D. Abell, D. A. Hoult, D. A. Bergman and D. P. Fairlie, *Bioorg. Med. Chem. Lett.*, 1997, **7**, 2853–2856.
34 F. Benedetti, F. Berti, S. Miertuš, D. Romeo, F. Schillani and A. Tossi, *Arkivoc*, 2003, 140–154.
35 R. Salto, L. M. Babe, J. Li, J. R. Rose, Z. H. Yu, A. Burlingame, J. J. De Voss, Z. H. Sui, P. R. Ortiz de Montellano and C. S. Craik, *J. Biol. Chem.*, 1994, **269**, 10691–10698.
36 X. Xie, T. Lemcke, R. Gussio, D. W. Zaharevitz, M. Leost, L. Meijer and C. Kunick, *Eur. J. Med. Chem.*, 2005, **40**, 655–661.
37 J. J. De Voss, Z. H. Sui, D. L. Decamp, R. Salto, L. M. Babe, C. S. Craik and P. R. Ortiz de Montellano, *J. Med. Chem.*, 1994, **37**, 665–673.
38 N. E. Kohl, E. A. Emini, W. A. Schleif, L. J. Davis, J. C. Heimbach, R. A. F. Dixon, E. M. Scolnick and I. S. Sigal, *Proc. Natl. Acad. Sci. U. S. A.*, 1988, **85**, 4686–4690.
39 J. Tang, *J. Biol. Chem.*, 1971, **246**, 4510–4517.
40 P. S. Caldera, Z. H. Yu, R. M. A. Knegtel, F. McPhee, A. L. Burlingame, C. S. Craik, I. D. Kuntz and P. R. Ortiz de Montellano, *Bioorg. Med. Chem.*, 1997, **5**, 2019–2027.
41 R. B. Rose, J. R. Rose, R. Salto, C. S. Craik and R. M. Stroud, *Biochemistry*, 1993, **32**, 12498–12507.
42 J. Mavri, *Int. J. Quantum Chem.*, 1998, **69**, 753–759.
43 B. Schiøtt and T. C. Bruice, *J. Am. Chem. Soc.*, 2002, **124**, 14558–14570.
44 K. H. Hopmann and F. Himo, *J. Phys. Chem. B*, 2006, **110**, 21299–21310.
45 K. H. Hopmann and F. Himo, *Chem.–Eur. J.*, 2006, **12**, 6898–6909.
46 K. H. Hopmann, B. M. Hallberg and F. Himo, *J. Am. Chem. Soc.*, 2005, **127**, 14339–14347.
47 E. Y. Lau, Z. E. Newby and T. C. Bruice, *J. Am. Chem. Soc.*, 2001, **123**, 3350–3357.
48 T. Laitinen, J. Rouvinen and M. Peräkylä, *J. Org. Chem.*, 1998, **63**, 8157–8162.
49 S. Gronert and J. M. Lee, *J. Org. Chem.*, 1995, **60**, 4488–4497.
50 H. Helten, T. Schirmeister and B. Engels, *J. Org. Chem.*, 2005, **70**, 233–237.
51 H. Helten, T. Schirmeister and B. Engels, *J. Phys. Chem. A*, 2004, **108**, 7691–7701.
52 S. Antoniotti, S. Antonczak and J. Golebiowski, *Theor. Chem. Acc.*, 2004, **112**, 290–297.
53 S. S. Glad and F. Jensen, *J. Chem. Soc., Perkin Trans. 2*, 1994, 871–876.
54 K. Omoto and H. Fujimoto, *J. Org. Chem.*, 2000, **65**, 2464–2471.
55 S. Okumoto and S. Yamabe, *J. Comput. Chem.*, 2003, **24**, 244–253.
56 J. Na, K. N. Houk, C. G. Shevlin, K. D. Janda and R. A. Lerner, *J. Am. Chem. Soc.*, 1993, **115**, 8453–8454.
57 G. P. Ford and C. T. Smith, *J. Am. Chem. Soc.*, 1987, **109**, 1325–1331.
58 S. I. Okovityi, E. L. Platitsyna and L. I. Kas'yan, *Russ. J. Org. Chem.*, 2001, **37**, 345–350.
59 S. Sirois, E. I. Proynov, J. F. Truchon, C. M. Tsoukas and D. R. Salahub, *J. Comput. Chem.*, 2003, **24**, 1110–1119.
60 Y. Xiang, D. W. Zhang and J. Z. H. Zhang, *J. Comput. Chem.*, 2004, **25**, 1431–1437.
61 C. C. J. Roothan, *Rev. Mod. Phys.*, 1951, **23**, 69–76.
62 W. J. Hehre, R. Ditchfield and J. A. Pople, *J. Chem. Phys.*, 1972, **56**, 2257.
63 P. C. Hariharan and J. A. Pople, *Mol. Phys.*, 1974, **27**, 209–214.
64 P. C. Hariharan and J. A. Pople, *Theor. Chim. Acta*, 1973, **28**, 213.
65 C. Møller and M. S. Plesset, *Phys. Rev.*, 1934, **46**, 618.
66 M. Head-Gordon, J. A. Pople and M. J. Frisch, *Chem. Phys. Lett.*, 1988, **153**, 503–506.
67 M. J. Frisch, M. Head-Gordon and J. A. Pople, *Chem. Phys. Lett.*, 1990, **166**, 275–280.
68 M. J. Frisch, M. Head-Gordon and J. A. Pople, *Chem. Phys. Lett.*, 1990, **166**, 281–289.
69 S. Saebo and P. Pulay, *Annu. Rev. Phys. Chem.*, 1993, **44**, 213–236.
70 S. Saebø and P. Pulay, *J. Chem. Phys.*, 1993, **98**, 2170–2175.
71 A. D. Becke, *J. Chem. Phys.*, 1993, **98**, 5648–5652.
72 C. T. Lee, W. T. Yang and R. G. Parr, *Phys. Rev. B*, 1988, **37**, 785–789.
73 B. Miehlich, A. Savin, H. Stoll and H. Preuss, *Chem. Phys. Lett.*, 1989, **157**, 200–206.
74 B. J. Lynch, P. L. Fast, M. Harris and D. G. Truhlar, *J. Phys. Chem. A*, 2000, **104**, 4811–4815.
75 B. J. Lynch and D. G. Truhlar, *J. Phys. Chem. A*, 2001, **105**, 2936–2941.
76 B. J. Lynch and D. G. Truhlar, *J. Phys. Chem. A*, 2002, **106**, 842–846.
77 Y. Zhao and D. G. Truhlar, *J. Phys. Chem. A*, 2005, **109**, 5656–5667.
78 Y. Zhao, N. E. Schultz and D. G. Truhlar, *J. Chem. Theory Comput.*, 2006, **2**, 364–382.
79 J. Zheng, Y. Zhao and D. G. Truhlar, *J. Chem. Theory Comput.*, 2007, **3**, 569–582.
80 Y. Zhao, N. E. Schultz and D. G. Truhlar, *J. Chem. Phys.*, 2005, **123**, 161103.
81 M. J. Frisch, G. W. Trucks, H. B. Schlegel, G. E. Scuseria, M. A. Robb, J. R. Cheeseman, J. A. Montgomery, Jr., T. Vreven, K. N. Kudin, J. C. Burant, J. M. Millam, S. S. Iyengar, J. Tomasi, V. Barone, B. Mennucci, M. Cossi, G. Scalmani, N. Rega, G. A. Petersson, H. Nakatsuji, M. Hada, M. Ehara, K. Toyota, R. Fukuda, J. Hasegawa, M. Ishida, T. Nakajima, Y. Honda, O. Kitao, H. Nakai, M. Klene, X. Li, J. E. Knox, H. P. Hratchian, J. B. Cross, V. Bakken, C. Adamo, J. Jaramillo, R. Gomperts, R. E. Stratmann, O. Yazyev, A. J. Austin, R. Cammi, C. Pomelli, J. W. Ochterski, P. Y. Ayala, K. Morokuma, G. A. Voth, P. Salvador, J. J. Dannenberg, V. G. Zakrzewski, S. Dapprich, A. D. Daniels, M. C. Strain, O. Farkas, D. K. Malick, A. D. Rabuck, K. Raghavachari, J. B. Foresman, J. V. Ortiz, Q. Cui, A. G. Baboul, S. Clifford, J. Cioslowski, B. B. Stefanov, G. Liu, A. Liashenko, P. Piskorz, I. Komáromi, R. L. Martin, D. J. Fox, T. Keith, M. A. Al-Laham, C. Y. Peng, A. Nanayakkara, M. Challacombe, P. M. W. Gill, B. Johnson, W. Chen, M. W. Wong, C. Gonzalez and J. A. Pople, *Gaussian*, Revision B.05, Gaussian, Inc., Pittsburgh PA, 2003.
82 *Jaguar, version 7.0*, Schrödinger, LLC, New York, NY, 2007.
83 E. Rutenber, E. B. Fauman, R. J. Keenan, S. Fong, P. S. Furth, P. R. Ortiz de Montellano, E. Meng, I. D. Kuntz, D. L. Decamp, R. Salto, J. R. Rose, C. S. Craik and R. M. Stroud, *J. Biol. Chem.*, 1993, **268**, 15343–15346.
84 T. Vreven, K. S. Byun, I. Komáromi, S. Dapprich, J. A. Montgomery, Jr., K. Morokuma and M. J. Frisch, *J. Chem. Theory Comput.*, 2006, **2**, 815–826.
85 S. Dapprich, I. Komáromi, K. S. Byun, K. Morokuma and M. J. Frisch, *THEOCHEM*, 1999, **462**, 1–21.
86 F. Maseras and K. Morokuma, *J. Comput. Chem.*, 1995, **16**, 1170–1179.
87 C. Y. Peng, P. Y. Ayala, H. B. Schlegel and M. J. Frisch, *J. Comput. Chem.*, 1996, **17**, 49–56.
88 D. J. Tannor, B. Marten, R. Murphy, R. A. Friesner, D. Sitkoff, A. Nicholls, M. Ringnalda, W. A. Goddard and B. Honig, *J. Am. Chem. Soc.*, 1994, **116**, 11875–11882.
89 B. Marten, K. Kim, C. Cortis, R. A. Friesner, R. B. Murphy, M. N. Ringnalda, D. Sitkoff and B. Honig, *J. Phys. Chem.*, 1996, **100**, 11775–11788.
90 C. P. Kelly, C. J. Cramer and D. G. Truhlar, *J. Chem. Theory Comput.*, 2005, **1**, 1133–1152.
91 K. E. Riley, B. T. Op't Holt and K. M. Merz, Jr., *J. Chem. Theory Comput.*, 2007, **3**, 407–433.
92 Y. Zhao and D. G. Truhlar, *J. Org. Chem.*, 2007, **72**, 295–298.
93 J. W. Schubert, T. J. Dudley and B. K. Ohta, *J. Org. Chem.*, 2007, **72**, 2452–2459.
94 P. R. Carlier, N. Deora and T. D. Crawford, *J. Org. Chem.*, 2006, **71**, 1592–1597.